Joint Uplink and Downlink EMF Exposure: Performance Analysis and Design Insights

Lin Chen, Ahmed Elzanaty, *Senior Member, IEEE*, Mustafa A. Kishk, *Member, IEEE*, Luca Chiaraviglio, *Senior Member, IEEE*, and Mohamed-Slim Alouini, *Fellow, IEEE*

***Abstract*— Installing more base stations (BSs) into the existing cellular infrastructure is an essential way to provide greater network capacity and higher data rates in the 5th-generation cellular networks (5G). However, a non-negligible amount of the population is concerned that such network densification will generate a notable increase in exposure to electric and magnetic fields (EMF) over the territory. In this paper, we analyze the downlink, uplink, and joint downlink&uplink exposure induced by the radiation from BSs and personal user equipment (UE), respectively, in terms of the received power density and exposure index. In our analysis, we consider the EMF restrictions set by the regulatory authorities such as the minimum distance between restricted areas (e.g., schools and hospitals) and BSs, and the maximum permitted exposure. Exploiting tools from stochastic geometry, mathematical expressions for the coverage probability and statistical EMF exposure are derived and validated. Tuning the system parameters such as the BS density and the minimum distance from a BS to restricted areas, we show a trade-off between reducing the population's exposure to EMF and enhancing the network coverage performance. Then, we formulate optimization problems to maximize the performance of the EMF-aware cellular network while ensuring that the EMF exposure complies with the standard regulation limits with high probability. For instance, the exposure from BSs is two orders of magnitude less than the maximum permissible level when the density of BSs is less than 20 BSs/km^2.**

***Index Terms*— Electric and magnetic fields exposure, stochastic geometry, coverage probability, Poisson hole process, EMF-aware cellular networks.**

Manuscript received 7 July 2022; revised 7 December 2022; accepted 6 February 2023. Date of publication 16 February 2023; date of current version 11 October 2023. The associate editor coordinating the review of this article and approving it for publication was C. Masouros. *(Corresponding author: Ahmed Elzanaty.)*

Lin Chen is with the Department of Information Engineering, The Chinese University of Hong Kong (CUHK), Hong Kong (e-mail: lin.chen@link.cuhk.edu.hk).

Ahmed Elzanaty is with the 5GIC & 6GIC, Institute for Communication Systems (ICS), University of Surrey, GU2 7XH Guildford, U.K. (e-mail: a.elzanaty@surrey.ac.uk).

Mustafa A. Kishk is with the Department of Electronic Engineering, Maynooth University, Maynooth, W23 F2H6 Ireland (e-mail: mustafa.kishk@mu.ie).

Luca Chiaraviglio is with the Department of Electronic Engineering, University of Rome "Tor Vergata," 00133 Rome, Italy, and also with the Consorzio Nazionale Interuniversitario per le Telecomunicazioni (CNIT), 43124 Parma, Italy (e-mail: luca.chiaraviglio@uniroma2.it).

Mohamed-Slim Alouini is with the CEMSE Division, KAUST, Thuwal 23955, Saudi Arabia (e-mail: slim.alouini@kaust.edu.sa).

Color versions of one or more figures in this article are available at https://doi.org/10.1109/TWC.2023.3244155.

Digital Object Identifier 10.1109/TWC.2023.3244155

I. Introduction

THE fundamental requirements of 5th-generation cellular network (5G) are low latency, high throughput, and wide coverage. One potential solution to accommodate 5G key performance indicators (KPIs) is to increase the number of base stations (BSs) [1]. The new 5G BSs inevitably act as additional radiation sources, concerning some of the population about the increasing possibility of their exposure to electric and magnetic fields (EMF). Recently, human health related to the massive deployment of BSs has raised public concerns [2]. There is an urgent need to provide scientific analysis as we do not know if health effects (not known at present time) will be observed in the future.

EMF exposure in cellular networks mainly comes from BSs and user equipment (UE), related to passive exposure and active exposure, respectively. BSs emit high power through long distances in the downlink, imposing EMF exposure to humans passively. The EMF exposure from all BSs in the network is usually measured by the power density at the user, which can be easily transformed into electric strength [3]. Nevertheless, the exposure originating from UE with low transmit power should also be taken into account due to the close distance between the user and the personal mobile device, which can be quantified by the received power density or the specific absorption rate (SAR) [4], [5]. In fact, EMF exposure associated with 5G radio frequency (RF) communications is considered as non-ionizing radiation that does not have enough energy to ionize the cells [6]. Nevertheless, the non-ionizing radiation is possible to generate heating effects in the exposed tissues, i.e., thermal effects [7], [8]. In order to guarantee that the thermal effects are below acceptable safe levels, EMF exposure guidelines are set such as those by International Telecommunication Union (ITU) [9], International Commission on Non-Ionizing Radiation Protection (ICNIRP) [4], and Federal Communications Commission (FCC) [10]. Each country has its own regulations on the safety limits to the EMF [11], [12], [13], [14], [15], mainly based on the aforementioned regulatory guidelines. Besides these guidelines, as a further precautionary measure, some countries adopt more restricted conditions such as a minimum distance between BSs and restricted areas, e.g., schools and hospitals [16]. Besides the well-understood thermal effects, there is a debate about whether long-term exposure to radiofrequency radiation (RFR) may have non-thermal effects that can lead to health

issues [17], [18]. Therefore, accurate analysis of the exposure to EMF is essential to permit designing EMF-aware cellular networks.

A. Related Work

In this subsection, we discuss the most related work on the EMF exposure, which can be divided into two categories: (i) EMF exposure assessment and (ii) EMF-aware network design.

1) EMF Exposure Assessment: The evaluation of EMF exposure in cellular networks can be conducted from experimental measurement and analytical points of view. As for the experimental measurement, the exposure induced by BSs and UEs was measured in [19], which revealed that the exposure from a personal mobile device could not be ignored. Considering the enabling technologies of 5G such as massive multiple-input multiple-output (MIMO), real-time beamforming, and high-frequency bands, 5G smartphones were used to capture the exposure level in a 5G network [20]. In [21], the distribution of EMF in 5G networks is investigated. The authors in [22] focused on the measurement of downlink exposure and showed that the exposure is well below the ICNIRP reference level. Clearly, the experimental measurement of EMF exposure illustrates the RFR level under a specific cellular network, while it is not able to explore the effect of the system parameters on EMF exposure for cellular network deployment.

As for the analytical evaluation of EMF exposure, authors in [23] considered a regular deployment of BSs under the assumption of a hexagonal mosaic territory. Employing stochastic geometry, more realistic modeling of irregularly distributed BSs was given in [24]. Compared with the experimental data of exposure in Brussels, Belgium, authors in [24] optimized the model parameters and verified the fitting effect of the proposed model. In [25], the statistical received power at users was used to monitor the downlink exposure levels in a MIMO system using tools from stochastic geometry. The above analytical modelling allows the prediction of the downlink EMF exposure from BSs before the actual network deployment. Yet, the uplink exposure from mobile equipment and EMF restrictions such as the minimum distance between BSs and restricted areas have not been considered in those analytical models. Thus, these models do not lead to an accurate evaluation of total EMF exposure in real cellular networks.

2) EMF-Aware Network Design: Recently, several researchers proposed novel cellular architectures to reduce EMF exposure or improve coverage performance while limiting the exposure [26]. Reconfigurable intelligent surfaces (RISs) were first proposed in [27] as a solution to create areas with reduced EMF. In [28], the RIS phases were optimized to minimize the total uplink exposure of users. On the other hand, the work in [29] and [30] considered designing the RIS phases to minimize the maximum exposure (min-max problem) with instantaneous and statistical channel state information, respectively. The authors in [31] applied probabilistic shaping to minimize the average EMF exposure while ensuring a target throughput. Considering the coexistence of macro-cell and small-cell BSs, the downlink EMF exposure and the coverage probability are studied in [32]. It is worth noting that the existing research on the EMF-aware network design mainly aims at mitigating the downlink/uplink EMF exposure on average and ensuring a target quality of service (QoS). Nevertheless, the total exposure (including downlink and uplink exposure) is rarely taken into account when designing the cellular network despite the fact that people are exposed to the RFR from both BSs and UEs [33]. Moreover, the regulation of restricted areas is seldom considered in the EMF-aware network design; while this regulation is essential for the evaluation of EMF exposure levels since the minimum distance between BSs and restricted areas can significantly reduce the exposure levels in restricted areas and can be selected by the system designers or decision makers. The effect of restricted areas on network performance has not been studied.

B. Contributions

In this paper, we provide a novel framework to analyze the impact of EMF exposure from both BSs and UE on the planning of a 5G cellular network from a statistical point of view. In particular, the proposed cellular network model considers the restrictions on the EMF exposure set by the regulatory authorities, including the maximum permitted EMF exposure and the exclusion zones around restricted areas, e.g., hospitals and schools [16]. Three scenarios are mainly studied in our model, including the downlink (passive exposure), the uplink (active exposure), and the joint downlink&uplink (passive and active exposure) RFR. Nevertheless, the inclusion of the restricted area, the maximum transmit power of the power with different channel inversion coefficients at UE, and the combination of the uplink and downlink lead to some mathematical challenges. These challenges are handled through approximations such as Poisson hole process (PHP), which are shown to be accurate through Monte Carlo simulations. The main contributions of our work are summarized as follows.

- We propose a stochastic geometry model that captures the minimum distance (R) between a BS and a restricted area. Specifically, restricted areas result in the PHP-distributed BSs. Such PHP approximation enables the following analysis of the effect of R on the exposure and coverage performance. The accuracy of the approximation has been validated in simulation.
- We quantify the downlink exposure from BSs and the uplink exposure from personal UE by the received power density under the Nakagami-m fading model. Correspondingly, we analyze the coverage probability in the downlink and uplink, respectively. Furthermore, considering a more practical scenario that the people are exposed to radiation from both BSs and UE, we provide the joint downlink&uplink exposure analysis, referred to as exposure index.
- We assess the compliance of cellular networks to the exposure guidelines. As opposed to the mean-value-based measurement of EMF exposure, our work provides the

cumulative distribution function (CDF) of exposure by using the Gil-Pelaez theorem. By comparing the 95-th percentile of EMF level with the standard limit defined by FCC, we ensure that the EMF exposure level complies with guidelines with a high probability.

- We design the system parameters, e.g., the density of the BSs and the minimum distance between the restricted areas and BSs, to *(i)* maximize the coverage performance constrained by the 95-th percentile of EMF exposure in the downlink and to *(ii)* minimize the joint downlink&uplink exposure. Numerical results show the impact of system parameters on network performance and exposure, and there exist optimal values of system parameters with respect to the minimal total exposure. These analyses provide insights into the design of future networks to meet the QoS and safety requirements.

The rest of the paper is structured as follows. Sec. II introduces the system model. The downlink analysis of the statistical EMF and SNR-based coverage probability are given in Sec. III, including the design of system parameters. Similar performance metrics in the uplink are presented in Sec. IV. Sec. V adopts the exposure index to account for the total influence of both uplink exposure and downlink exposure on the population. Then, the simulation results are shown and discussed in Sec. VI. Finally, Sec. VII concludes the paper.

II. System Model

This section describes the considered system of a cellular network with the EMF-deployment constraint and corresponding stochastic geometry-based model.

We investigate a network composed of BSs and UEs, which are equipped with omnidirectional antennas. In fact, the case of directional antennas can be handled under the proposed framework with the scaled density of BSs and antenna gain [34]. Particularly, the deployment of BSs complies with the EMF regulation on the minimum distance between BSs and the restricted areas (such as schools and hospitals). As shown in Fig. 1(a), there are several restricted areas surrounded by exclusion zones/holes where BSs are not allowed (by EMF regulation) to be deployed [16]. The radius of the exclusion zones/holes, denoted by R, can be regarded as the minimum distance between BSs and the restricted areas. Using tools from stochastic geometry, the locations of BSs and users are generally assumed to follow two independent homogeneous PPPs [35]. However, considering the exclusion zones around restricted areas, we propose to model the locations of the BSs as a PHP. The PHP is generated using two independent PPPs:

1) the baseline PPP $\Psi_b \equiv \{b_i\} \subset \mathbb{R}^2$ with density λ_b.
2) the PPP modeling the locations of the restricted areas, which represent the centers of the exclusion zones (i.e., holes), $\Psi_r \equiv \{r_i\} \subset \mathbb{R}^2$ with density λ_r.

Therefore, the locations of the BSs construct a PHP Ψ_B, formally defined as follows

$$\Psi_B = \left\{ b_i \in \Psi_b : b_i \notin \bigcup_{r_i \in \Psi_r} \mathcal{B}(r_i, R) \right\}, \tag{1}$$

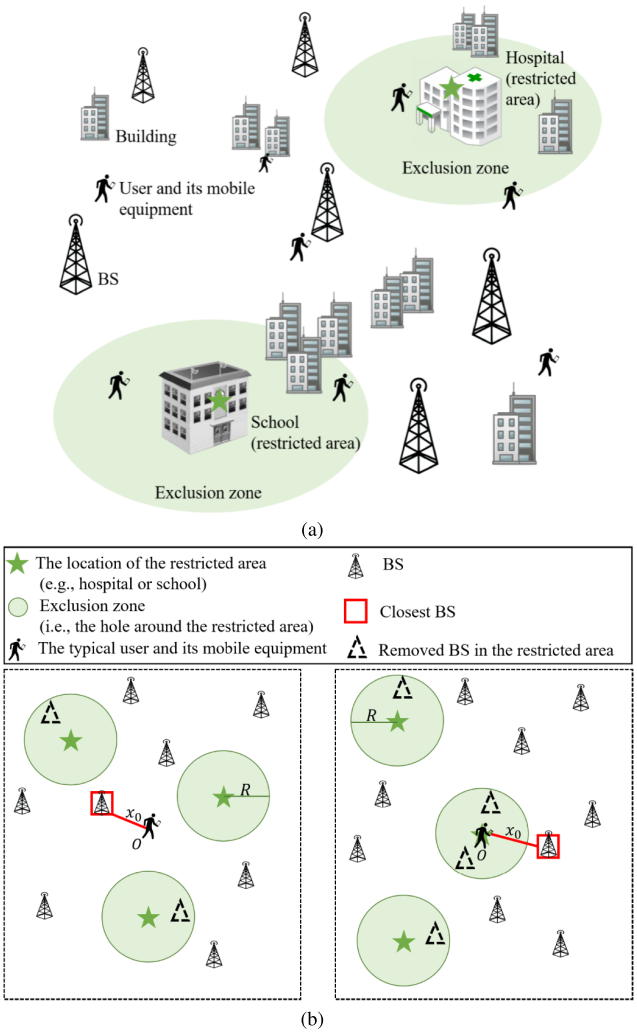

Fig. 1. A cellular network considering the restricted areas. (a) a general scenario (b) geometric representation (left: the typical user outside the exclusion zone, right: the typical user inside the exclusion zone).

where $\mathcal{B}(r_i, R)$ is an exclusion zone/hole, a disk centered at r_i with radius R. The density of Ψ_B can be approximated as

$$\lambda_B = \lambda_b \exp(-\lambda_r R^2). \tag{2}$$

Fig. 1(b) presents a realization of PHP-distributed BSs, marked by triangles with solid black borders. BSs that fall in the exclusion zones (i.e. green circles) are removed and become dashed triangles. Besides, a BS only serves a single UE in each time-frequency recourse block. The nearest association rule is considered for the connection between BSs and users, i.e., a user is connected with its nearest BS. Without loss of generality, we focus on the analysis for a typical user located at the origin of the network [36]. Due to the limitation of the restricted areas, the location of the typical user (inside/outside the exclusion zone) impacts its performance. Therefore, in the following, we distinguish the analysis of the typical user in two different locations: outside or inside the exclusion zone, as shown in Fig. 1(b).

III. EMF-Aware Downlink Exposure

In this section, the downlink performance metrics are derived to characterize the statistics of the EMF exposure, the

TABLE I
TABLE OF NOTATIONS

Notation	Description
Ψ_b	The Poisson point process (PPP) modeling the baseline locations of the BSs
Ψ_r	The PPP modeling the locations of the restricted areas
Ψ_B	The PHP modeling the locations of BSs affected by restricted areas
λ_b; λ_r; λ_B	The density of Ψ_b; Ψ_r; Ψ_B
α; β	The value of the path-loss exponent for calculating signal-to-noise ratio (SNR); EMF exposure
$p_{\max}$	The maximum transmit power in the uplink
j	$j=\sqrt{-1}$ is the imaginary unit
$\mathrm{SAR}^{\mathrm{UL}}$; $\mathrm{SAR}^{\mathrm{DL}}$	The value of SAR in the uplink; downlink

coverage probability, and the allowable distance between a BS and a user. Then, we formulate an optimization problem to maximize the downlink coverage probability subject to the EMF exposure constraint.

A. Performance Metrics: Downlink Exposure and Coverage

The downlink EMF exposure is quantified by the received power density from all BSs over the territory. Following the system model discussed in Sec. II, the output power of a BS is

$$p = P_t G_t, \tag{3}$$

where P_t is the transmit power of the BS and G_t is the antenna gain. Based on the Friis law, the received power at the typical user from a BS with horizontal distance x_i is given by

$$P_{\mathrm{rec}}(x_i) = \frac{p\, G_u\, \eta\, H_i}{(x_i^2+h^2)^{\beta/2}}, \tag{4}$$

where G_u is the user's antenna gain, $\eta = (\frac{c/f}{4\pi d_0})^2$ represents the path loss at reference distance $d_0 = 1$ m (with frequency f and wave speed $c = 3\times 10^8$ m/s), h is the height of BSs, β is the path-loss exponent, and H_i is the small-scale fading gain with an expected value of 1, i.e., $\mathbb{E}\{H_i\} = 1$. More specifically, we adopt the widely-used Nakagami-m fading model (with shaping parameters given by m) to characterize the small-scale fading. The probability density function (PDF) of H_i is given by [37]

$$f_{H_i}(\omega) = \frac{m^m \omega^{m-1}}{\Gamma(m)} e^{-m\omega}, \tag{5}$$

where $\Gamma(m) = \int_0^\infty t^{m-1}e^{-t}\mathrm{d}t$ is the Gamma function [38]. The corresponding received power density can be expressed as

$$W(x_i) = \frac{P_{\mathrm{rec}}(x_i)}{A_e} = \frac{pH_i}{4\pi(x_i^2+h^2)^{\beta/2}}, \tag{6}$$

where $A_e = \frac{(c/f)^2 G_u}{4\pi}$ is the antenna effective area of the typical user. Since the BS height is negligible compared with the horizontal distance x_i, for simplicity, the Euclidean distance between a BS and the typical user is approximated as their horizontal distance in the rest of the paper. Hence, for the typical user located at the origin, the downlink EMF exposure is

$$W^{\mathrm{DL}} = \sum_{i, b_i\in\Psi_B} \frac{pH_i}{4\pi x_i^{\beta}}. \tag{7}$$

For this setup, our objective is to ensure that the value of W^{DL} is below the maximum allowed value by regulatory authorities with a high probability [39], [40]. In particular, the below condition (termed downlink EMF constraint) is required to be satisfied

$$\mathbb{P}(W^{\mathrm{DL}} \le W_{\max}) \ge \rho, \tag{8}$$

where $W_{\max}$ is the maximum power density specified by the guidelines. The value of ρ can be chosen as 0.95, according to the assessment of compliance regulation by ITU [39]. This is opposed to the deterministic approaches where W^{DL} is not considered as a random variable (r.v.), and it should be strictly less than $W_{\max}$, i.e., $\rho \equiv 1$ [41].

From (4), when the typical user associates with its closest BS with a distance of x_0, the received power in the downlink can be expressed as

$$P_{\mathrm{rec}}^{\mathrm{DL}}(x_0) = \frac{p\eta H_0}{x_0^{\alpha}}, \tag{9}$$

where the BS height is ignored, G_u is assumed to be 1, and α is the path-loss exponent. The instantaneous SNR in the downlink is given by

$$\mathrm{SNR}^{\mathrm{DL}} = \frac{P_{\mathrm{rec}}^{\mathrm{DL}}(x_0)}{\sigma^2} = \frac{p\eta H_0}{x_0^{\alpha}\sigma^2}, \tag{10}$$

where σ^2 is noise power, and H_0 is the small-scale fading following (5). Note that the path-loss exponent is represented by two different notations, i.e., α and β, for calculating the EMF exposure and SNR, respectively, which enables us to analyze the worst case and the typical case by setting different relations between α and β. For a given value of λ_B, the downlink coverage probability can be defined as follows,

$$\mathcal{P}_{\mathrm{cov}}^{\mathrm{DL}}(\lambda_B) = \mathbb{P}(\mathrm{SNR}^{\mathrm{DL}} > \tau), \tag{11}$$

where τ is a predefined threshold.

B. Performance Analysis

This subsection provides several steps to derive the mathematical expressions for the performance metrics formally defined in Sec. III-A from the perspective of the typical user outside or inside the hole, respectively. For instance, considering that BSs are excluded from the exclusion zones, the distance between the typical user located in the restricted area and its nearest BS must be larger than the radius of the exclusion zone.

1) Distance Distribution to the Closest BS: Let $X_{\rm out}$ and $X_{\rm in}$ denote the distance from the typical user to its closest BS given that the user is outside or inside the hole, respectively. The following lemma presents the distribution of the contact distances $X_{\rm out}$ and $X_{\rm in}$.

Lemma 1: The PDF of the distance between the typical user and the closest BS is denoted by

$$f_{X_{\rm out}}(x) = 2\pi\lambda_B x \exp\left(-\lambda_B \pi x^2\right), x \geq 0, \tag{12a}$$

$$f_{X_{\rm in}}(x) = \begin{cases} 2\pi\lambda_B x \exp\left(-\lambda_B\pi(x^2-R^2)\right), & \text{if } x \geq R \\ 0 & \text{, if } x < R, \end{cases} \tag{12b}$$

where $\lambda_B = \lambda_b \exp(-\lambda_r R^2)$, (12a) is for the user outside the hole, and (12b) is for the user inside the hole.

Proof: See Appendix A. □

2) Coverage Probability: The probability that SNR is above a predefined threshold, i.e., the complementary cumulative distribution function (CCDF) of SNR, is used as a metric to describe QoS of the cellular network. Based on the distance distribution of $X_{\rm out}$ and $X_{\rm in}$, we develop the expression of the downlink coverage probability relative to a SNR threshold τ.

Theorem 1: The downlink coverage probability of the typical user served by its closest BS is

$$\mathcal{P}_{\rm cov}^{\rm DL} = \int_0^\infty \sum_{k=0}^{m-1} \frac{(s^{\rm DL}\sigma^2)^k}{k!} \exp\left(-s^{\rm DL}\sigma^2\right) f_{X_v}(x_0)\,{\rm d}x_0,$$
$$s^{\rm DL} = \frac{m\tau}{p\eta x_0^{-\alpha}},\ v \in \{\text{in}, \text{out}\}, \tag{13}$$

where v represents whether or not the typical user is in a restricted area.

Proof: See Appendix B. □

3) EMF Constraint: The EMF exposure is required to be below the maximum allowed value ($W_{\max}$) by the authority regulations with a high probability (ρ). (8) can be rewritten in terms of the CDF of the downlink power density, i.e., $F_{W^{\rm DL}}(w)$, as

$$F_{W^{\rm DL}}(W_{\max}) \geq \rho. \tag{14}$$

Therefore, the EMF constraint can be expressed as

$$F_{W^{\rm DL}}^{-1}(\rho) \leq W_{\max}, \tag{15}$$

where $F_{W^{\rm DL}}^{-1}(\rho)$ is the inverse function of $F_{W^{\rm DL}}(w)$.

Theorem 2: The CDF of the downlink EMF exposure is given by

$$F_{W^{\rm DL}}(w) = \frac{1}{2} - \frac{1}{2j\pi}\int_0^\infty \frac{1}{t} \times \left[e^{-jtw}\mathcal{L}_{W^{\rm DL}}(-jt) - e^{jtw}\mathcal{L}_{W^{\rm DL}}(jt)\right]{\rm d}t, \tag{16}$$

where $\mathcal{L}_{W^{\rm DL}}(s)$ is the Laplace transform of downlink EMF exposure and

$$\mathcal{L}_{W^{\rm DL}}(s) = \exp\left(-2\pi\lambda_B \int_{v(R)}^\infty \left[1-\kappa^{\rm DL}(x,s)\right] x\,{\rm d}x\right),$$
$$\kappa^{\rm DL}(x,s) = \left(\frac{m}{m + sp(4\pi)^{-1}x^{-\beta}}\right)^m, \tag{17}$$

where R is the radius of the hole, λ_B is the density of PHP-distributed BSs, and $v(R) = 0$ if the typical user is outside the hole, otherwise $v(R) = R$.

Proof: See Appendix C. □

4) Compliance Distance Between Users and BSs: The distance between a BS and a user should comply with the EMF constraint, i.e., conditioned on the serving BS located at a compliance distance x_c to the typical user, the corresponding conditional EMF exposure should not exceed the maximum allowable limit ($W_{\max}$) with a high probability (ρ). Namely, x_c satisfies the conditional EMF constraint as follows,

$$F_{W^{\rm DL}|X_{\rm out}=x_c}(W_{\max}) \geq \rho, \tag{18}$$

where $F_{W^{\rm DL}|X_{\rm out}=x_c}(W_{\max})$ is the CDF of the downlink EMF exposure conditioned on the distance between the serving BS and the user being x_c. The minimum value of x_c that satisfies (18) is denoted by $x_{\rm com}$ and is given by

$$x_{\rm com} \triangleq \inf_{x\in\mathbb{R}} \left\{x : F_{W^{\rm DL}|X_{\rm out}=x}(W_{\max}) \geq \rho\right\}. \tag{19}$$

No public access is allowed to the area centered at a BS with the radius of $x_{\rm com}$, since people inside will experience downlink EMF exposure above the safety threshold.

Theorem 3: The CDF of the EMF exposure conditioned on the serving BS being at a distance x_0 from the typical user is given by

$$F_{W^{\rm DL}|x_0}(w) = \frac{1}{2} - \frac{1}{2j\pi}\int_0^\infty \frac{1}{t}\Big[e^{-jtw}\mathcal{L}_{W^{\rm DL}|x_0}(-jt) - e^{jtw}\mathcal{L}_{W^{\rm DL}|x_0}(jt)\Big]{\rm d}t, \tag{20}$$

where $\mathcal{L}_{W^{\rm DL}|x_0}(s)$ is the Laplace transform of conditional EMF exposure and

$$\mathcal{L}_{W^{\rm DL}|x_0}(s) = \kappa^{\rm DL}(x_0,s)\exp\left(-2\pi\lambda_B\int_{x_0}^\infty \left[1-\kappa^{\rm DL}(x,s)\right]x\,{\rm d}x\right), \tag{21}$$

where λ_B is given in (2) and $\kappa^{\rm DL}(\cdot)$ is given in (17).

Proof: See Appendix D. □

When setting $w = W_{\max}$ and ρ as a constant defined by the ITU, $F_{W^{\rm DL}|x_0}(w)$ is a function of x_0. Using its inverse

function, we can find the minimum compliance distance between a user and a BS, $x_{\rm com}$. Thus, the compliance distance is $x_c \geq x_{\rm com}$.

C. Optimal EMF-Aware Design

We try to maximize the downlink coverage probability while ensuring that the downlink EMF constraint is always satisfied. This optimization problem can be formally defined as follows,

$$\mathbf{OP_1}: \underset{\lambda_B \in \mathbb{Z}_+}{\text{maximize}} \ \mathcal{P}_{\rm cov}^{\rm DL}(\lambda_B) \quad \text{subject to:} \ \mathbb{P}(W^{\rm DL} \leq W_{\max}) \geq \rho. \tag{22}$$

Intuitively, the network would have better coverage performance as the BS density λ_B increases since the distance between the typical user and its closest BS becomes closer and the path loss is correspondingly reduced, thereby improving the downlink SNR. However, the EMF exposure is expected to increase, which means the optimal density λ_B^* (corresponding to a specific baseline density of BSs, λ_b^*) can be found by gradually increasing the value of λ_B until $F_{W^{\rm DL}}^{-1}(\rho, \lambda_B^*)$ reaches $W_{\max}$. Based on (2), increasing λ_B can be realized by reducing the density and the radius of holes or increasing the baseline density.

IV. EMF-Aware Uplink Exposure

In this section, we focus on the EMF exposure induced by individual mobile equipment. We define the uplink performance metrics and then provide a corresponding analysis.

A. Performance Metrics: Uplink Exposure and Coverage

We now analyze the uplink exposure of the cellular network described in Sec. II. The mobile equipment deploys a power control mechanism on its transmit power to compensate for the path loss, fully or partially depending on the power control factor ϵ, i.e., $\epsilon = 1$ and $0 < \epsilon < 1$, respectively. The transmit power at the mobile equipment can be defined as

$$P_{\rm tran}^{\rm UL}(x_0) = \begin{cases} p_u x_0^{\alpha\epsilon}, & x_0 < X_{\max} \\ p_{\max}, & \text{otherwise}, \end{cases} \quad \epsilon \in (0,1], \tag{23}$$

where p_u is a constant, α is the path-loss exponent, x_0 is the distance between the BS and its serving user, $p_{\max}$ is the maximum transmit power of the mobile equipment, and $X_{\max} = (p_{\max}/p_u)^{1/\alpha\epsilon}$. Let u_0 denote the distance from the user to its personal mobile equipment and assume that u_0 is in the far-filed of the transmit antenna of mobile equipment.[1] The distance from the BS to its associated user or mobile equipment is assumed to be equivalent since the distance from the typical user to its own mobile device is much shorter than that to its serving BS, i.e., $u_0 \ll x_0$. Unlike the downlink exposure that comes from all BSs in the network, the uplink exposure is dominated by the user's personal mobile equipment [42], [43]. Specifically, the transmit power at mobile equipment is quite low and attenuates significantly after long-distance transmission. Therefore, the exposure from other users' mobile devices to the typical user is negligible. However, due to the close distance between the typical user and his own mobile device, the corresponding exposure can not be ignored. Thus, the uplink EMF exposure at the typical user can be assessed by the received power density from its mobile equipment (termed as typical UE) as

$$W^{\rm UL}(x_0) = \frac{P_{\rm tran}^{\rm UL}(x_0)\Omega}{4\pi u_0^\beta} = \begin{cases} \dfrac{p_u x_0^{\alpha\epsilon}\Omega}{4\pi u_0^\beta}, & x_0 < X_{\max} \\ \dfrac{p_{\max}\Omega}{4\pi u_0^\beta}, & \text{otherwise}, \end{cases} \tag{24}$$

where x_0 is the distance between the typical user and its serving BS (termed as tagged BS) and Ω follows the Nakagami-m fading in (5) with mean 1. The uplink EMF exposure is also required to be below the maximum permitted value by regulatory authorities with a high probability of ρ, i.e., the uplink EMF constraint can be expressed as

$$\mathbb{P}(W^{\rm UL} \leq W_{\max}) \geq \rho. \tag{25}$$

The received power at the tagged BS from the typical UE with a distance x_0 is given by

$$P_{\rm rec}^{\rm UL}(x_0) = \frac{P_{\rm tran}^{\rm UL}(x_0)\eta\Omega_0}{x_0^\alpha} = \begin{cases} p_u x_0^{\alpha(\epsilon-1)}\eta\Omega_0, & x_0 < X_{\max} \\ \dfrac{p_{\max}\eta\Omega_0}{x_0^\alpha}, & \text{otherwise}, \end{cases} \tag{26}$$

where Ω_0 is the small-scale fading and has the same distribution as Ω, and η is defined in (4). In particular, if $\epsilon = 1$, it is a full power control case, and the average received power will be a constant when $x_0 < X_{\max}$.

The corresponding instantaneous SNR in the uplink can be expressed as

$$\text{SNR}^{\rm UL} = \frac{P_{\rm rec}^{\rm UL}(x_0)}{\sigma^2}, \tag{27}$$

which can be used to compute the uplink coverage probability as follows

$$\mathcal{P}_{\rm cov}^{\rm UL}(\lambda_B) = \mathbb{P}(\text{SNR}^{\rm UL} > \tau), \tag{28}$$

where λ_B is givn in (2) and τ is the predefined threshold.

B. Performance Analysis

Similar to the downlink case, we analyze the uplink exposure of the typical user inside and outside the hole, respectively, and the uplink coverage probability. The distribution of the distance between the typical user and its closest BS in Lemma 1 is still applicable to the following analysis.

1) Coverage Probability: The following theorem gives the expression of the coverage probability under the power control mechanism, which is defined as the CCDF of the uplink SNR.

[1]Nowadays, the smartphone is not used as a plain old telephone attached to the ear, but rather it is put in front of the chest and used for, e.g., chatting, exploring social media, watching videos, or listening to streaming audio.

Theorem 4: The uplink coverage probability of the users inside or outside the hole is given by

$$\mathcal{P}_{\text{cov}}^{\text{UL}} = \int_0^{X_{\max}} \sum_{k=0}^{m-1} \frac{(s_1^{\text{UL}}\sigma^2)^k}{k!} \exp\left(-s_1^{\text{UL}}\sigma^2\right) f_{X_v}(x_0)\,\mathrm{d}x_0 + \int_{X_{\max}}^{\infty} \sum_{k=0}^{m-1} \frac{(s_2^{\text{UL}}\sigma^2)^k}{k!} \exp\left(-s_2^{\text{UL}}\sigma^2\right) f_{X_v}(x_0)\,\mathrm{d}x_0, \tag{29}$$

where $v \in \{\text{in}, \text{out}\}$, $s_1^{\text{UL}} = \frac{m\tau}{p_u x_0^{\alpha(\epsilon-1)}\eta}$, $s_2^{\text{UL}} = \frac{m\tau}{p_{\max}\eta x_0^{-\alpha}}$, *and* $f_{X_v}(x_0)$ *is given in (12).*

Proof: Similar to the method in Appendix C. □

2) EMF Constraint: The uplink EMF exposure at the typical user is mostly from its own mobile equipment, which should be lower than the maximum allowed value by authority regulations with a high probability. Similar to the downlink EMF constraint, (25) can be derived from the Laplace transform of the uplink received power density, denoted by $\mathcal{L}_{W^{\text{UL}}}$ as

$$\mathcal{L}_{W^{\text{UL}}}(s) = \int_0^{X_{\max}} \kappa_1^{\text{UL}}(x_0, s) f_{X_v}(x_0)\,\mathrm{d}x_0 + \int_{X_{\max}}^{\infty} \kappa_2^{\text{UL}}(s) f_{X_v}(x_0)\,\mathrm{d}x_0, \tag{30}$$

where u_0 is the distance between the typical user and its mobile equipment, $f_{X_v}(x_0)$ is defined in Lemma 1, $v \in \{\text{in}, \text{out}\}$, $\kappa_1^{\text{UL}}(x_0, s) = \left(\frac{m}{m + s p_u x_0^{\alpha\epsilon}(4\pi)^{-1} u_0^{-\beta}}\right)^m$, and $\kappa_2^{\text{UL}}(s) = \left(\frac{m}{m + s p_{\max}(4\pi)^{-1} u_0^{-\beta}}\right)^m$.

Theorem 5: The CDF of the uplink EMF exposure is given by

$$F_{W^{\text{UL}}}(w) = \frac{1}{2} - \frac{1}{2j\pi}\int_0^{\infty} \frac{1}{t}\left[e^{-jtw}\mathcal{L}_{W^{\text{UL}}}(-jt) - e^{jtw}\mathcal{L}_{W^{\text{UL}}}(jt)\right]\mathrm{d}t. \tag{31}$$

Therefore, the uplink EMF constraint can be described by the inverse function of $F_{W^{\text{UL}}}(w)$, i.e., $F^{-1}_{W^{\text{UL}}}(\rho) \le W_{\max}$.

From the above analysis, we notice that, under the power control mechanism, the closer distance between the user and its serving BS leads to lower transmit power at its UE. Unlike what we discussed in Sec. III-C, increasing the number of BSs is beneficial for both the reduction of the exposure and the improvement of the coverage probability in the uplink. Therefore, the uplink optimization problem is omitted.

V. Joint Downlink&Uplink Exposure

In most situations, a person is exposed to EMF from both his/her own mobile equipment and BSs. In this section, we consider a metric called exposure index that accounts for both the uplink and downlink exposure in the cellular network discussed in Sec. II, followed by the performance analysis and the optimal EMF-aware network design.

A. Performance Metrics: Exposure Index

In [44], a metric that quantifies the population exposure to EMF is introduced. This metric considers both the uplink and downlink EMF exposure. It also accounts for user-specific properties such as age (adult or child), usage (data or voice call), and posture (standing or sitting). The total exposure (termed exposure index) at the typical user can be expressed as the sum of uplink exposure index (EI^{UL}) and downlink exposure index (EI^{DL}), which is given by [44]

$$\begin{aligned}\text{EI}(x_0) &= \text{EI}^{\text{UL}}(x_0) + \text{EI}^{\text{DL}} \\ &= \text{SAR}^{\text{UL}} P_{\text{tran}}^{\text{UL}}(x_0) + \text{SAR}^{\text{DL}} W^{\text{DL}} \\ &= \text{SAR}^{\text{UL}} P_{\text{tran}}^{\text{UL}}(x_0) + \text{SAR}^{\text{DL}} \sum_{i, b_i \in \Psi_B} \frac{pH_i}{4\pi x_i^{\beta}} \\ &\quad [\text{W/kg}],\end{aligned} \tag{32}$$

where x_0 is the distance between the typical user and the serving BS located ar b_0, $P_{\text{tran}}^{\text{UL}}$ is the uplink transmit power defined in (23), W^{DL} is the downlink received power density defined in (7), SAR^{UL} is the reference induced SAR in the uplink when the transmit power from the UE is unity, and SAR^{DL} is the reference induced SAR in the downlink when the received power density from the BS at the UE is unity. More clearly, $\text{SAR}^{\text{UL}}\left[\frac{\text{W}}{\text{kg}}/\text{W}\right]$ is normalized to unit transmit power and $\text{SAR}^{\text{DL}}\left[\frac{\text{W}}{\text{kg}}/\frac{\text{W}}{\text{m}^2}\right]$ is normalized to unit power density. It is worth noting that the reference SAR depends on the user-specific properties mentioned earlier.

B. Performance Analysis

The exposure index in (32) can be divided into two parts, i.e., one is related to the serving BS at b_0 with distance x_0 and the other is from the rest of BS, as follows.

$$\text{EI}(x_0) = \left(\text{SAR}^{\text{UL}} P_{\text{tran}}^{\text{UL}}(x_0) + \text{SAR}^{\text{DL}} \frac{pH_0}{4\pi x_0^{\beta}}\right) + \text{SAR}^{\text{DL}} \sum_{i, b_i \in \Psi_B \setminus \{b_0\}} \frac{pH_i}{4\pi x_i^{\beta}}. \tag{33}$$

The Laplace transform of the exposure index $\text{EI}(x_0)$ conditioned on x_0 is given by

$$\mathcal{L}_{\text{EI}|x_0}(s) = \exp\left(-s\text{SAR}^{\text{UL}} P_{\text{tran}}^{\text{UL}}(x_0)\right)\kappa^{\text{J}}(x_0, s) \times \exp\left(-2\pi\lambda_B \int_{x_0}^{\infty} \left[1 - \kappa^{\text{J}}(x, s)\right] x\,\mathrm{d}x\right), \tag{34}$$

where $\kappa^{\text{J}}(x_0, s) = \left(\frac{m}{m + s\text{SAR}^{\text{DL}} p (4\pi)^{-1} x_0^{-\beta}}\right)^m$.

Proof: The Laplace transform of $\text{EI}(x_0)$ in (33) is given by (35), shown at the bottom of the next page. Then, we process (35) by following the similar approaches in Appendix D and thus obtain (34). □

Based on the distance distribution of x_0 in Lemma 1, the unconditional Laplace transform of the exposure index can be obtained as

$$\mathcal{L}_{\text{EI}}(s) = \int_0^{\infty} \mathcal{L}_{\text{EI}|x_0}(s) f_{X_v}(x_0)\,\mathrm{d}x_0, \tag{36}$$

where $f_{X_v}(x_0)$ is given in (12). Additionally, the Laplace transform of $\mathrm{EI}^{\mathrm{UL}}$ and $\mathrm{EI}^{\mathrm{DL}}$ can be expressed as

$$\begin{aligned}\mathcal{L}_{\mathrm{EI}^{\mathrm{UL}}}(s) =&\mathbb{E}\left[\exp\left(\mathrm{SAR}^{\mathrm{UL}}P^{\mathrm{UL}}_{\mathrm{tran}}(x_0)\right)\right]\\ =&\int_0^{\infty}\exp\left(-s\mathrm{SAR}^{\mathrm{UL}}P^{\mathrm{UL}}_{\mathrm{tran}}(x_0)\right)f_{X_v}(x_0)\,\mathrm{d}x_0,\end{aligned} \tag{37a}$$

$$\begin{aligned}\mathcal{L}_{\mathrm{EI}^{\mathrm{DL}}}(s) =&\mathbb{E}\left[\exp\left(\mathrm{SAR}^{\mathrm{DL}}W^{\mathrm{DL}}\right)\right]\\ =&\exp\left(-2\pi\lambda_B\int_{v(R)}^{\infty}\left[1-\kappa^J(x,s)\right]x\,\mathrm{d}x\right),\end{aligned} \tag{37b}$$

where (37a) is from $\mathbb{E}[g(t)]=\int_0^{\infty}g(t)f_T(t)\mathrm{d}t$, $f_T(t)$ is the PDF of t, and (37b) can be obtained by following the similar methods to Appendix C. Based on the Gil-Pelaez theorem in (46), we derive the CDF of EI in the following theorem.

Theorem 6: The CDF of the total exposure including the uplink exposure and the downlink exposure (i.e. exposure index) is given by

$$F_{\mathrm{EI}}(\varepsilon)=\frac{1}{2}-\frac{1}{2j\pi}\int_0^{\infty}\frac{1}{t}\left[e^{-jt\varepsilon}\mathcal{L}_{\mathrm{EI}}(-jt)-e^{jt\varepsilon}\mathcal{L}_{\mathrm{EI}}(jt)\right]\mathrm{d}t. \tag{38}$$

C. Optimal EMF-Aware Design

As we mentioned before, increasing the density of BSs is effective to enhance the coverage performance both in the downlink and uplink and reduce the uplink EMF exposure. On the contrary, increasing the density of BSs has a negative influence on the downlink EMF exposure. Therefore, the proper design of λ_B is essential to minimize both the uplink and downlink exposure. In the following, we formulate an optimization problem to find the optimal density of BSs that minimizes EI in (33) (that quantifies the joint downlink&uplink exposure). Since EI is a random variable, we optimize its ρ-th percentile as follows

$$\mathbf{OP_3}: \underset{\lambda_B\in\mathbb{Z}_+}{\text{minimize}} \quad F^{-1}_{\mathrm{EI}}(\rho,\lambda_B), \tag{39}$$

where F^{-1}_{EI} is the inverse CDF of EI. The optimal λ_B^* can be found by any efficient one dimension search algorithm such as bi-sectional [45] or golden section methods [46]. Based on (2), λ_B^* is corresponding to a specific baseline density of BSs, λ_b^*, and a specific radius of the exclusion zone, R^*.

VI. Numerical Results and Discussion

In this section, Monte Carlo simulations and numerical results for the analytical expressions are conducted.

TABLE II
Table of System Numerical Parameters

System Parameters	Default Values
λ_r; λ_b	10^{-6} holes/m^2; 10^{-5} BSs/m^2
α; β	4; 2.5
f	2600 MHz
η	-40 dB
G_t	15 dB
P_t	200 W
p_u	0.008 mW
$p_{\max}$	200 mW
ϵ	0.4
m	1
u_0	20 cm
R	50 m
σ^2(downlink; uplink)	10^{-11} W; 10^{-12} W
$\mathrm{SAR}^{\mathrm{UL}}$; $\mathrm{SAR}^{\mathrm{DL}}$	0.0053 $\frac{\mathrm{W}}{\mathrm{kg}}$/W; 0.0042 $\frac{\mathrm{W}}{\mathrm{kg}}/\frac{\mathrm{W}}{\mathrm{m}^2}$

The performance of the EMF-aware cellular network is investigated for three scenarios, i.e., the downlink, uplink, and joint downlink&uplink. The parameters used in numerical results and their default values are given in Table. II. Some of them are swept to explore their effects on the EMF exposure and coverage probability. Without loss of generality, we consider the Nakagami-m fading with $m=1$.

A. Worst-Case Scenario for Downlink Exposure

The downlink simulations are firstly conducted under the conservative setting, where we consider the maximum transmit power (200 W) and the maximum antenna gain (15 dB) at 5G BSs [27, Table 6]. Based on the recommendation provided in 3GPP TR 36.814–900 [47], as a conservative setting, the path-loss exponent is set as $\alpha=4$ while analyzing the downlink coverage probability (by considering that the communication link is blocked) and as $\beta=2.5$ while computing the downlink EMF exposure (for the environment free of blockages).

In Fig. 2, we compare the statistical exposure level inside and outside the restricted area for different minimum allowable distances between the BS and restricted areas, R. In particular, the statistical level, denoted by $F^{-1}_{W^{\mathrm{DL}}}(\rho)$, means that the exposure will not exceed this level with a high probability of ρ, as explained in (15). According to the compliance regulations [39], we set $\rho=0.95$, and $F^{-1}_{W^{\mathrm{DL}}}(0.95)$ represents the 95-th percentile of exposure level in the downlink. The EMF exposure level without considering the minimum distance

$$\begin{aligned}\mathcal{L}_{\mathrm{EI}|x_0}(s) &= \mathbb{E}_{\mathrm{EI}}\left[\exp(-s\mathrm{EI}(x_0))\right]\\ &= \mathbb{E}_{\mathrm{EI}}\left[\exp\left[-s\left(\mathrm{SAR}^{\mathrm{UL}}P^{\mathrm{UL}}_{\mathrm{tran}}(x_0)+\mathrm{SAR}^{\mathrm{DL}}\frac{pH_0}{4\pi x_0^{\beta}}\right)-s\left(\mathrm{SAR}^{\mathrm{DL}}\sum_{i,b_i\in\Psi_B\setminus\{b_0\}}\frac{pH_i}{4\pi x_i^{\beta}}\right)\right]\right]\\ &= \exp(-s\mathrm{SAR}^{\mathrm{UL}}P^{\mathrm{UL}}_{\mathrm{tran}}(x_0))\mathbb{E}_{H_0}\left[\exp\left(-s\mathrm{SAR}^{\mathrm{DL}}\frac{pH_0}{4\pi x_0^{\beta}}\right)\right]\mathbb{E}_{\Psi_B,\{H_i\}}\left[\prod_{i,b_i\in\Psi_B\setminus\{b_0\}}\exp\left(-s\mathrm{SAR}^{\mathrm{DL}}\frac{pH_i}{4\pi x_i^{\beta}}\right)\right].\end{aligned} \tag{35}$$

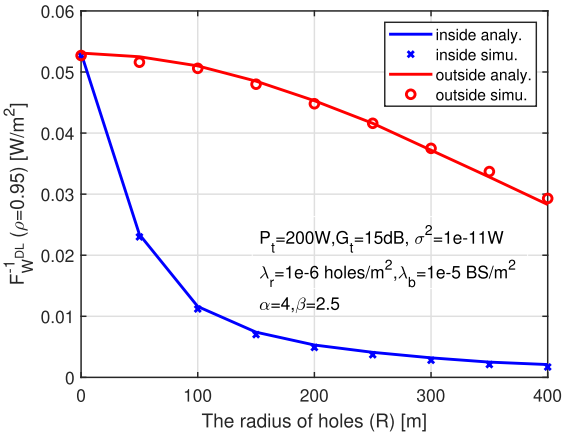

Fig. 2. The 95-th percentile of exposure level in the downlink (i.e., power density induced at the typical user) inside or outside the restricted area for various exclusion zone radii.

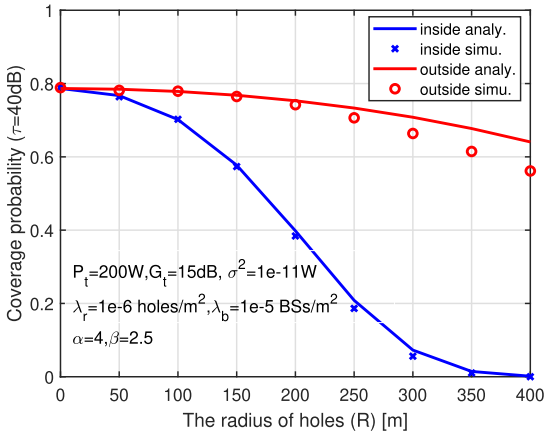

Fig. 3. Focusing on $\tau = 40$ dB, the CCDF of the downlink SNR levels inside or outside the restricted area for various exclusion zone radii.

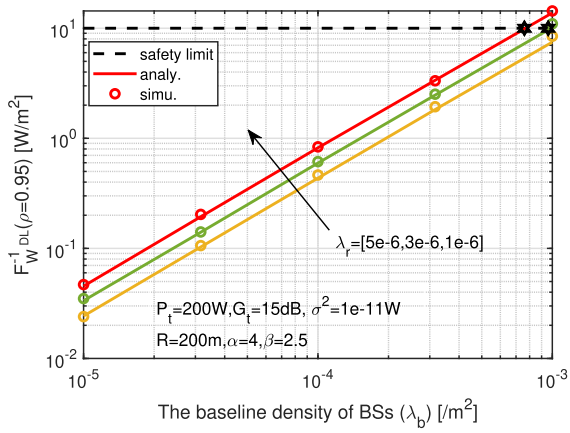

Fig. 4. The 95-th percentile of exposure level in the downlink outside the restricted area vs the baseline density of the BSs, for various densities of the restricted areas.

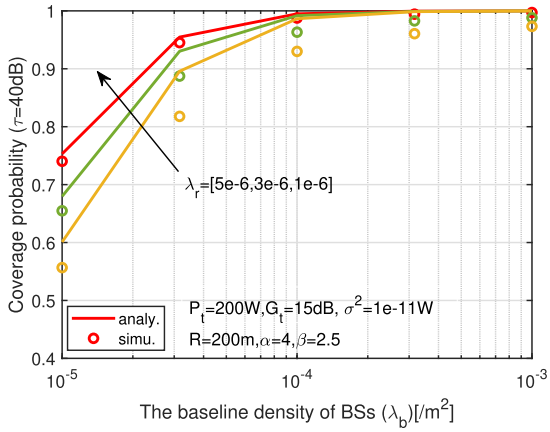

Fig. 5. The CCDF of the downlink SNR levels outside the restricted area vs baseline densities of BSs, for various densities of the restricted areas.

between BSs and restricted areas (i.e., the hole radius $R = 0$ m) has been studied in [4] and [12]. It can be observed from Fig. 2 that the regulation on the minimum distance between BSs and restricted areas greatly affects the measurement of EMF exposure. Obviously, the exposure of the typical user outside the hole is higher than the one inside the restricted area, as the distance between the BS and the typical user in the restricted area is always larger than the hole radius R. Moreover, Fig. 2 illustrates that a rise in the radius of the hole dramatically reduces the exposure for the user inside the hole and still has a slight impact on the user outside the hole. This is because a larger value of R not only leads to the longer propagation distance but slightly decreases the density of BSs in (2), resulting in fewer BSs, namely, fewer radiating sources.

In Fig. 3, the coverage probability is depicted against the hole radius, for the same settings considered in Fig. 2. We notice that the typical user outside the restricted areas experiences better coverage than the user inside. We can also observe a slight reduction in the coverage of the users outside the restricted areas as we increase the hole radius (for similar reasons as explained in our comments on Fig. 2). By comparing Fig. 2 and Fig. 3, it is noticed that the hole with a large radius can protect people from serious EMF exposure while impairing communication quality. It is also worth noting that at larger values of R, the gap between simulation and analytical results is caused by the PHP approximation of the BS distribution.

Fig. 4 and Fig. 5 show the impact of the density of the restricted areas/holes (λ_r) and the baseline density of the BSs (λ_b) on the EMF exposure and coverage probability, respectively, for the users outside the restricted areas. Since the holes ensure a lower exposure level in the restricted areas than that outside the hole, the safety requirement of the user inside the hole can be guaranteed as long as the EMF exposure of the user outside the hole is less than the maximum allowable value ($W_{\max} = 10$ W/m^2, depicted as the dashed horizontal line) defined by the FCC [39]. We see that both the exposure and coverage probability decrease for higher values of λ_r, while densely deployed BSs favourably affect coverage probability but adversely affect EMF exposure in the downlink. The reason is that with the increasing BS density, the serving BS may be closer to the typical user, and thus SNR would be improved. However, the dense deployment of BSs would increase the radiating sources, making the typical user more likely to be exposed to higher electromagnetic radiation levels. In particular, the maximum density (identified by the star-shaped markers in Fig. 4) corresponds to the maximum allowable exposure. This maximum density is analyzed in the following paragraph.

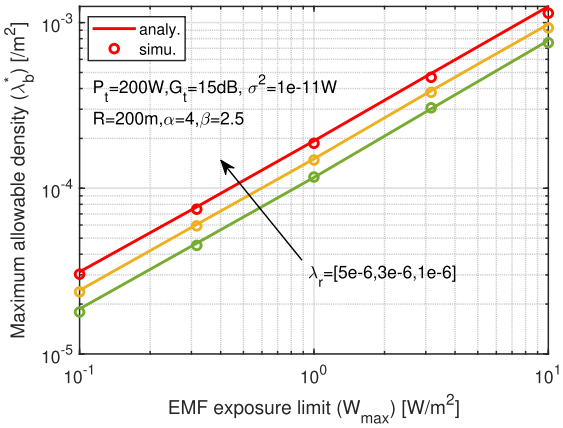

Fig. 6. The maximum allowable baseline density λ_b^* for different regulations on the maximum allowed EMF exposure.

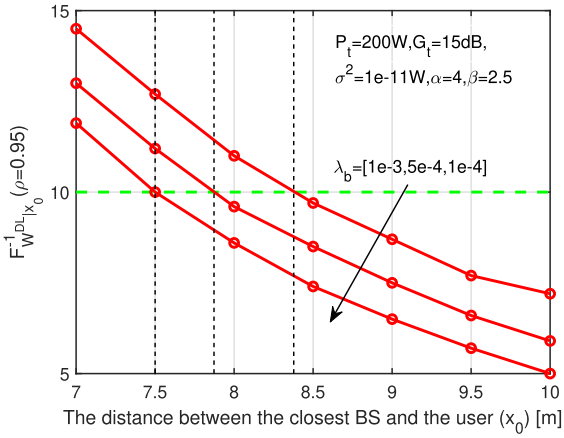

Fig. 7. The 95-th percentile of exposure level in the downlink conditioned on the closest BS at x_0.

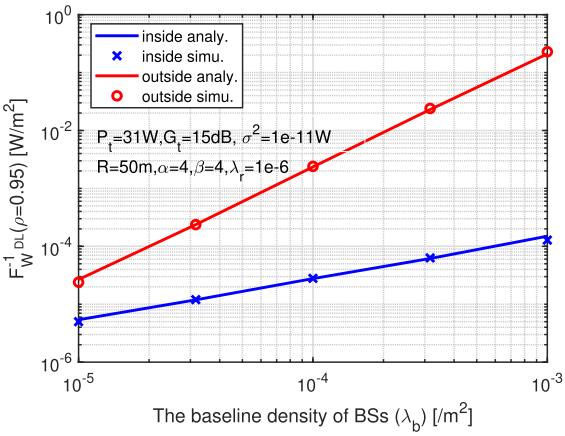

Fig. 8. The 95-th percentile of exposure level in the downlink under the practical setting.

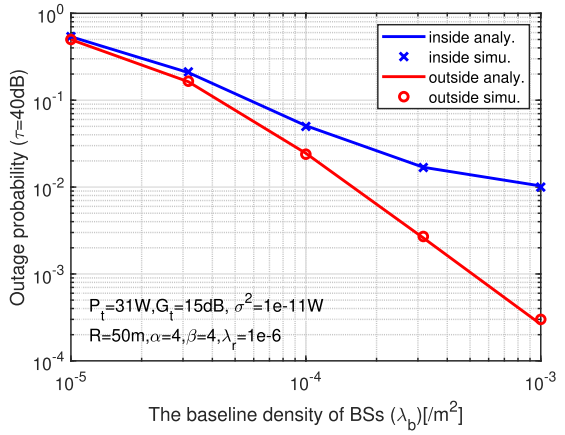

Fig. 9. Compared with $\tau = 40$ dB, the outage probability in the downlink under the practical setting.

In Fig. 6, we depict the maximum allowable baseline density λ_b^*, obtained by solving the optimization problem in (22), vs various levels of maximum permitted EMF exposure, for different values of λ_r. For example, considering the FCC limit on the power density, 10 $\mathrm{W/m^2}$, the optimal value of λ_b maximizes the downlink coverage probability is 7.6×10^{-4} $\mathrm{BSs/m^2}$, for $\lambda_r = 10^{-6}$ $\mathrm{holes/m^2}$ and $R = 200$ m.

In Fig. 7, we plot the 95-th percentile of exposure level conditioned on the distance from the typical user to its closest BS being at x_0 to calculate the compliance distance between users and BSs. As mentioned in Sec. III-B.4, compared with the FCC limits (depicted as the dashed horizontal line), the minimum compliance distance between a BS and a user, x_{com}, can be found. For the cellular network with $\lambda_b = 10^{-4}$ $\mathrm{BSs/m^2}$ and $\lambda_r = 10^{-6}$ $\mathrm{holes/m^2}$, x_{com} is 7.5 m, which satisfies $F_{W^{\mathrm{DL}}|7.5}(10) = 0.95$. Namely, public safety cannot be ensured if they enter an area centered at a BS with a radius of x_{com}.

B. Typical-Case Scenario for Downlink Exposure

The results in a more common case are given in Fig. 8 and Fig. 9, where a statistical reduction factor of 0.31 is applied to the general downlink transmit power (100 W), i.e. $P_t = 100$ W $\times$ 0.31 [27, Table 6] and the same path-loss exponent ($\alpha = \beta = 4$) is used for evaluating the network performance in the downlink. Fig. 8 suggests that the 95-th percentile of exposure level in such a typical case is far below the FCC limit even in a network with the intensive deployment of BSs. This observation supports the conception that the development of network densification will not trigger severe health problems. In Fig. 9, instead of giving the coverage probability, we plot the outage probability, the probability of an outage event when the SNR cannot meet the required threshold, and we see that the simulation results closely match the analysis results.

C. Uplink Exposure

In the uplink, fractional power control at the UE is considered which makes the transmit power a function of the distance to the associated BS. The maximum transmit power at the UE is set to 200 mW (i.e., the maximum transmit power in 5G mobile equipment [27, Table 6]). The distance between the user and its personal mobile equipment is assumed to be in far field of the UE antenna with $u_0 = 20$ cm. [2] Since the close

[2]The far field of the antenna is defined as $u > \frac{2D^2}{c/f}$, where D is the diameter of the antenna and c/f is the wavelength of the uplink frequency f. Considering the Long Term Evolution (LTE) using a frequency band of 2600 MHz, $D = 10$ cm, and $c/f = (3 \times 10^8$ m/s$)/(2600$ MHz), we have $u > 17.3$ cm. Thus, $u_0 = 20$ cm satisfies the far-field condition of the UE's antenna [44].

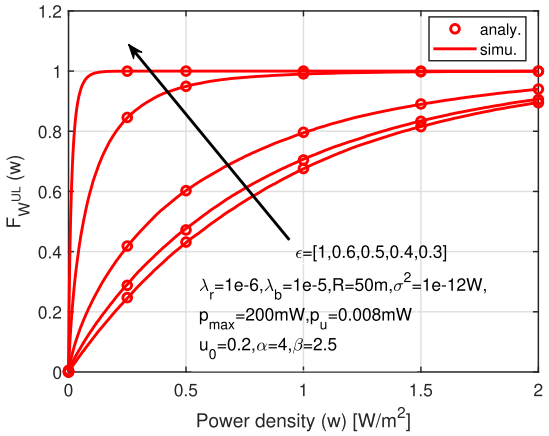

Fig. 10. The CDF of uplink power density levels outside the restricted area for various power control factors.

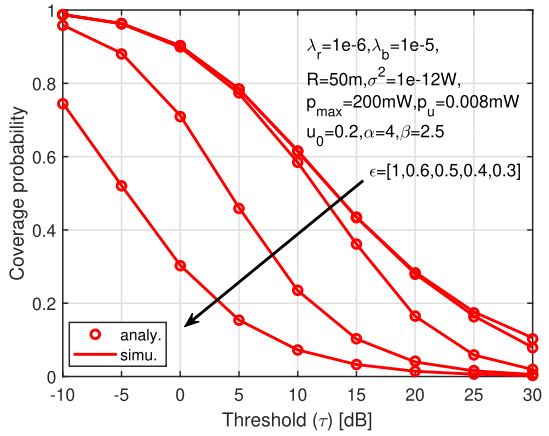

Fig. 11. The CCDF of the uplink SNR levels outside the restricted area for various power control factors.

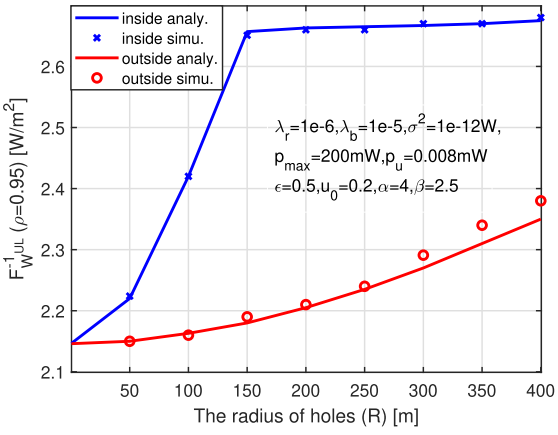

Fig. 12. The 95-th percentile of exposure level in the uplink inside or outside the restricted area for various exclusion zone radii.

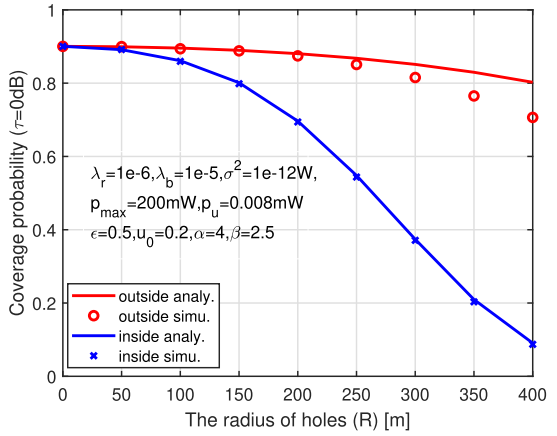

Fig. 13. The CCDF of the uplink SNR levels inside or outside the restricted area for various exclusion zone radii.

distance between the user and its personal mobile equipment, the path-loss exponent (β) between them is typically smaller than that (α) between the mobile equipment and its serving BS. Thus, we set $\alpha = 4$ and $\beta = 2.5$. Besides, lower noise power is considered since the frequency band in uplink is normally narrower than that in downlink.

The impact of power control factor ϵ on the distribution of uplink EMF exposure and SNR is presented in Fig. 10 and Fig. 11, respectively. It can be seen from Fig. 10 that increasing the power control factor ϵ leads to more severe exposure in uplink. This is because the transmit power of UE with the distance-proportional power control increases with ϵ, as shown in (23). Similarly, in Fig. 11, the larger the power control factor, the higher power the serving BS receives, thereby enhancing the coverage performance. Intuitively, as we increase ϵ up to 1, the transmit power can completely compensate the path loss in the BS-UE link and the received power will equal to p_u if the distance between a BS and its serving user (x_0) is below $X_{\max}$ (as described in Sec. IV-A). However, if x_0 exceeds $X_{\max}$, then $P^{\mathrm{UL}}_{\mathrm{tran}}$ reaches its maximum value of 200 mW, which explains the small difference in Fig. 10 and Fig. 11 when changing ϵ from 0.6 to $\epsilon = 1$.

In Fig. 12 and Fig. 13, we explore the effect of hole radius R on the exposure level and the coverage probability in the uplink. Different from simulation results on the downlink exposure in Sec. VI-A, in Fig. 12, the user inside the hole is exposed to higher-level RFR emitted from personal mobile equipment than the user outside the hole. Interestingly, we notice that increasing the zone radius R does not mitigate RFR for both two kinds of users (inside and outside the holes). The reason for this anomaly is that we control the transmit power at UE, which is monotonically increasing with the distance between the user and its serving BS as in (23). Particularly, for the user outside the hole, when we expand R, the density of PHP-distributed BSs, λ_B, will decrease. The reduced number of BSs has no effect on uplink radiating sources since the uplink exposure is induced by an individual's mobile device. However, the distance between the closest BS to the typical user may become farther, resulting in stronger transmit power at UE and exposure to the user. We also notice that the uplink exposure level of the typical user inside the hole gradually tends to be constant when $R > 150$ m, which is the consequence of maximum transmit power constraint. On the other hand, the uplink coverage probability decreases as we increase the hole radius, as shown in Fig. 13. This trend is similar to the downlink scenario observed in Fig. 3.

Next, we discuss the influence of λ_b on the network performance metrics in Fig. 14 and Fig. 15. Increasing the value of λ_b leads to a decrease in the 95-th percentile of EMF exposure (as shown in Fig. 14) and an increase in coverage probability (as shown in Fig. 15) for the typical user inside and outside the restricted area. In fact, after increasing the baseline density

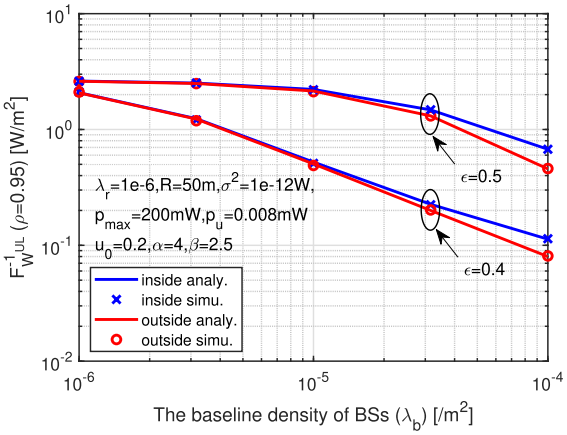

Fig. 14. The 95-th percentile of exposure level in the uplink inside or outside the restricted area vs various baseline densities of BSs for different values of power control factor.

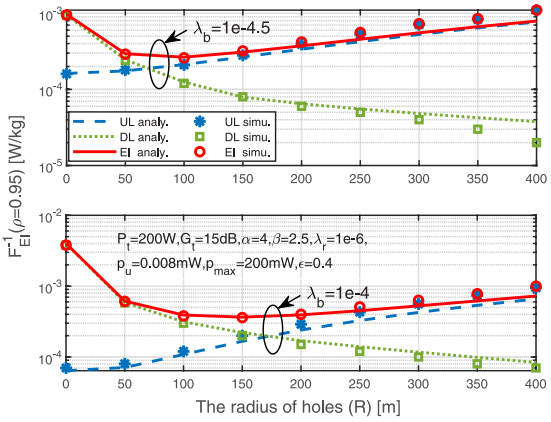

Fig. 16. The 95-th percentile of exposure level of EI, EI^{UL} and EI^{DL} inside the restricted area vs various exclusion zone radii for different λ_b.

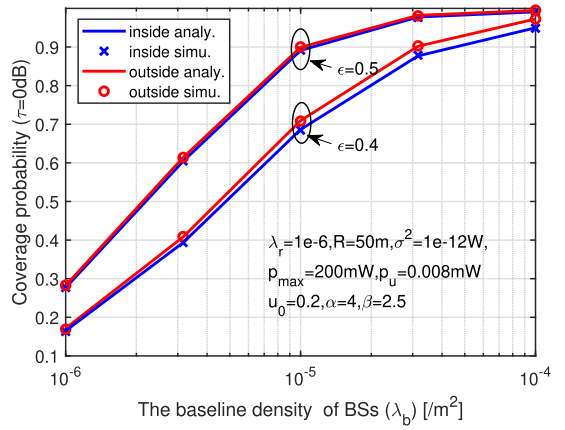

Fig. 15. The CCDF of the uplink SNR levels inside or outside the restricted area vs various baseline densities of BSs for different values of power control factor.

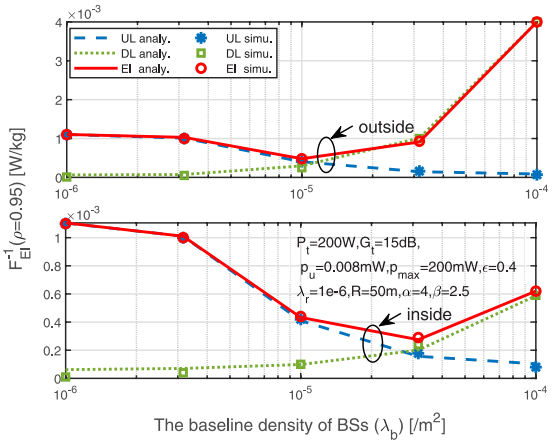

Fig. 17. The 95-th percentile of exposure level of EI, EI^{UL} and EI^{DL} inside or outside the restricted area vs various baseline densities of BSs.

λ_b, there are more BSs around the typical user, which has the potential to reduce the distance (x_0) between the typical user and its serving BS. Meanwhile, the shorter distance x_0 leads to lower transmit power in (23) and lower EMF exposure levels in (24). The improvement in coverage probability and the mitigation in EMF exposure in uplink reveals that dense deployment of BSs is conducive to the future cellular network design.

D. Exposure Index (Joint Downlink&Uplink Exposure)

Generally, the SAR value of voice usage is larger than that of other usages, such as data downloading/ uploading. Considering such a worst case, we choose $\text{SAR}^{\text{UL}} = 0.0053$, and $\text{SAR}^{\text{DL}} = 0.0042$ [44, Table 27].

Fig. 16 reveals the impact of hole radius on the joint downlink&uplink exposure. It can be concluded from Fig. 2 and Fig. 12 that the existence of holes around the restricted areas cannot mitigate the exposure from UE but it is effective for reducing the exposure from BSs. The contradicting trend (between the increase in uplink exposure and the decrease in downlink exposure when expanding the exclusion zone radius) reminds us that we cannot blindly protect the users by removing BSs near the restricted areas, which also causes both uplink and downlink coverage performance degradation as can be seen in Fig. 3 and Fig. 13. Therefore, Fig. 16 considers joint downlink and uplink exposure as EI when resizing the hole radius. In Fig. 16, when $R < 100$ m, the total exposure is mainly from the BSs in downlink but when $R \geq 100$ m, downlink exposure is gradually decreasing and uplink exposure becomes dominant. Namely, there exists an optimal value, e.g., $R^* = 100$ m, that minimizes the total exposure for the network with $\lambda_b = 10^{-4.5}$ BSs/m^2.

In Fig. 17, we plot the 95-th percentile of EI for the typical user inside and outside the restricted area under different baseline densities of BSs. The dense deployment of BSs can improve both uplink and downlink coverage probability as shown in Fig. 5 and Fig. 15. Nevertheless, the uplink and downlink exposure levels show opposite trends with the increase of the baseline density λ_b, as shown in Fig. 4 and Fig. 14, respectively. These imply that there is an optimal value of λ_b that minimizes the EI, i.e., a solution to the optimization problem in (39). For the typical user inside the hole, it can be observed from Fig. 17 that there is a turning point $\lambda_b^* = 10^{-4.5}$ BSs/m^2. Before this point, EI is dominated by EI^{UL}, and after it, EI is dominated by EI^{DL}. At this point, the joint exposure, EI, at the restricted area is minimized. For the typical user outside the hole, the optimal baseline density, λ_b^*, corresponding to the minimum EI is 10^{-5} BSs/m^2.

VII. Conclusion

This paper integrated the EMF restrictions on the coverage performance and exposure analysis and formulated optimization problems on how to design the EMF-aware cellular networks. Particularly, the distribution of BSs was generated by a PHP, accounting for the distance between BSs and restricted areas where the presence of BSs is prohibited. Using tools of stochastic geometry, we analyzed the radiation and coverage probability in terms of downlink and uplink. Furthermore, we investigated the effect of system parameters on the joint downlink&uplink radiation from both BSs and UE through EI. With the aid of numerical results, we showed that even the conservative evaluation of the 95-th percentile of EMF exposure level can still comply with the international guidelines, and the exposure in more typical settings is far below the maximum permissible level. It can also be seen that increasing the baseline density of BSs or decreasing the permitted distance around restricted areas can reduce the exposure from mobile equipment in uplink while exacerbating the exposure from BSs in downlink. Such opposite trend demonstrated the reasonability of taking joint downlink&uplink exposure into account when designing the system parameters for the EMF-aware cellular network. We found that there exists optimal values of the distance between restricted areas and BSs and the baseline density of BSs that minimizes the total exposure under a certain network configuration.

Appendix A
Proof of Lemma 1

The PHP Ψ_B can be approximated as a PPP with density $\lambda_B = \lambda_b \exp(-\lambda_r R^2)$. Following the standard result of PPP [48], the Lebesgue measure of the area centered at the typical user outside the hole can be expressed as $\rho_{\text{out}}(x) = \pi x^2, x \geq 0$. Using the null probability of PPP in [49], the CDF of X_{out} is given by

$$\begin{aligned} F_{X_{\text{out}}}(x) &= \mathbb{P}\left\{X_{\text{out}} \leq x\right\} \\ &= 1 - \mathbb{P}\left\{X_{\text{out}} > x\right\} \\ &= 1 - \exp\left[\lambda_B \rho_{\text{out}}(x)\right] \\ &= 1 - \exp(-\lambda_B \pi x^2) \\ &= 1 - \exp\left[-\lambda_b \exp(-\lambda_r R^2)\pi x^2\right]. \end{aligned} \tag{40}$$

Because of the relationship between PDF and CDF, i.e., $f_{X_{\text{out}}}(x) = \frac{\mathrm{d}}{\mathrm{d}x} F_{X_{\text{out}}}(x)$, we can obtain the PDF of X_{out}, $f_{X_{\text{out}}}(x)$, in (12a). For the typical user inside the hole, the Lebesgue measure of the area is given by $\rho_{\text{in}}(x) = \pi(x^2 - R^2), x \geq R$, where R is the radius of the holes. Then, using the same steps of deriving $f_{X_{\text{out}}}(x)$, we finish the proof of $f_{X_{\text{in}}}(x)$.

Appendix B
Proof of Theorem 1

We start by analyzing the downlink coverage probability of the typical user outside the hole. With the distribution of X_{out} in (12a), (10) and (11) can be further processed as

$$\begin{aligned} \mathcal{P}_{\text{cov}}^{\text{DL}} &= \mathbb{P}\left\{\text{SNR}^{\text{DL}} > \tau\right\} \\ &= \mathbb{E}_{X_{\text{out}}}\left[\mathbb{P}\left\{\text{SNR}^{\text{DL}} > \tau | X_{\text{out}}\right\}\right] \\ &= \int_0^\infty \mathbb{P}\left\{\text{SNR} > \tau | X_{\text{out}} = x_0\right\} f_{X_{\text{out}}}(x_0)\,\mathrm{d}x_0 \\ &= \int_0^\infty \mathbb{P}\left\{\frac{p\eta H_0}{x_0^\alpha \sigma^2} > \tau\right\} f_{X_{\text{out}}}(x_0)\,\mathrm{d}x_0. \end{aligned} \tag{41}$$

From the distribution of H_0 in (5), we have

$$\begin{aligned} \mathbb{P}\left\{\frac{p\eta H_0}{x_0^\alpha \sigma^2} > \tau\right\} &= \mathbb{P}\left\{H_0 > \frac{\tau \sigma^2}{p\eta x_0^{-\alpha}}\right\} \\ &= \frac{\Gamma_u\left(m, s^{\text{DL}}\sigma^2\right)}{\Gamma(m)} \\ &\overset{(a)}{=} \sum_{k=0}^{m-1} \frac{(s^{\text{DL}}\sigma^2)^k}{k!} \exp\left(-s^{\text{DL}}\sigma^2\right), \end{aligned} \tag{42}$$

where $\Gamma_u(m, mg) = \int_{mg}^\infty t^{m-1} e^{-t}\,\mathrm{d}t$, $s^{\text{DL}} = \frac{m\tau}{p\eta x_0^{-\alpha}}$ and (a) is from the definition $\frac{\Gamma_u(m,g)}{\Gamma(m)} = \exp(-g)\sum_{k=0}^{m-1}\frac{g^k}{k!}$. Taking (42) into (41), we obtain the expression of $\mathcal{P}_{\text{cov}}^{\text{DL}}$ for the typical user outside the hole. The proof of $\mathcal{P}_{\text{cov}}^{\text{DL}}$ for the typical user inside the hole is similar to the above approach, which therefore is omitted here.

Appendix C
Proof of Theorem 2

In order to find the CDF of EMF exposure in the downlink, we first derive the Laplace transform of W^{DL}, which is given by

$$\begin{aligned} \mathcal{L}_{W^{\text{DL}}}(s) &= \mathbb{E}_{W^{\text{DL}}}\left[\exp(-sW^{\text{DL}})\right] \\ &= \mathbb{E}_{W^{\text{DL}}}\left[\exp\left(-s\sum_{i,b_i\in\Psi_B}\frac{pH_i}{4\pi x_i^\beta}\right)\right] \\ &= \mathbb{E}_{\Psi_B}\left[\prod_{i,b_i\in\Psi_B}\mathbb{E}_H\left[\exp\left(-s\frac{pH}{4\pi x_i^\beta}\right)\right]\right] \\ &\overset{(a)}{=} \mathbb{E}_{\Psi_B}\left[\prod_{i,b_i\in\Psi_B}\kappa^{\text{DL}}(x_i, s)\right], \end{aligned} \tag{43}$$

where $\kappa^{\text{DL}}(x_i, s) = \left(\frac{m}{m + sp(4\pi)^{-1}x_i^{-\beta}}\right)^m$ and (a) is from the distribution of small-scale fading H in (5). Focusing on the typical user outside the hole and employing the probability generating functional (PGFL) of PPP in [35], (43) can be further expressed as

$$\mathcal{L}_{W^{\text{DL}}}(s) = \exp\left(-2\pi\lambda_B\int_0^\infty\left[1 - \kappa^{\text{DL}}(x, s)\right]x\mathrm{d}x\right), \tag{44}$$

where $\lambda_B = \lambda_b \exp(-\lambda_r R^2)$. While for the user inside the hole, $x_i \geq R$ and thus the Laplace transform of W^{DL} is

$$\mathcal{L}_{W^{\text{DL}}}(s) = \exp\left(-2\pi\lambda_B\int_R^\infty\left[1 - \kappa^{\text{DL}}(x, s)\right]x\,\mathrm{d}x\right). \tag{45}$$

From Gil-Pelaez theorem, the CDF of W^{DL} can be written as

$$\begin{aligned} F_{W^{\text{DL}}}(w) &= \frac{1}{2} - \frac{1}{\pi}\int_0^\infty \frac{1}{t}\,\text{Im}\left(\exp(-j\,t\,w)\phi_{W^{\text{DL}}}(t)\right)\mathrm{d}t \\ &= \frac{1}{2} - \frac{1}{\pi}\int_0^\infty \frac{1}{t}\,\text{Im}\left(\exp(-j\,t\,w)\mathcal{L}_{W^{\text{DL}}}(-j\,t)\right)\mathrm{d}t \end{aligned}$$

$$= \frac{1}{2} - \frac{1}{2j\pi}\int_0^\infty \frac{1}{t}\left[e^{-j\,t\,w}\mathcal{L}_{W^{\mathrm{DL}}}(-j\,t) - e^{j\,t\,w}\mathcal{L}_{W^{\mathrm{DL}}}(j\,t)\right]\mathrm{d}t, \tag{46}$$

where $\phi_{W^{\mathrm{DL}}}(t) = \mathbb{E}\{\exp(j\,t\,w)\} = \mathcal{L}_{W^{\mathrm{DL}}}(-j\,t)$. Submitting (44) or (45) into (46), we prove Theorem 2.

Appendix D
Proof of Theorem 3

Under the condition that the serving BS is located at b_0 with distance x_0 to the typical user, the power density received at the typical user is from the closest BS with a distance of x_0 and from the rest of BSs with distances greater than x_0 to the typical user, which is given by

$$W^{\mathrm{DL}}(x_0) = \frac{pH_0}{4\pi x_0^\beta} + \sum_{i,b_i\in\Psi_B\setminus\{b_0\}} \frac{pH_i}{4\pi x_i^\beta}. \tag{47}$$

The Laplace transform of $W^{\mathrm{DL}}(x_0)$ is given by

$$\begin{aligned}\mathcal{L}_{W^{\mathrm{DL}}|x_0}(s) &= \mathbb{E}_{W^{\mathrm{DL}}|x_0}\left[\exp\left(-s\frac{pH_0}{4\pi x_0^\beta} - s\sum_{i,b_i\in\Psi_B\setminus\{b_0\}}\frac{pH_i}{4\pi x_i^\beta}\right)\right]\\ &= \mathbb{E}_{H_0}\left[\exp(-s\frac{pH_0}{4\pi x_0^\beta})\right] \times \mathbb{E}_{\Psi_B,\{H_i\}}\left[\prod_{i,b_i\in\Psi_B\setminus\{b_0\}}\exp\left(-s\frac{pH_i}{4\pi x_i^\beta}\right)\right]\\ &\overset{(a)}{=} \kappa^{\mathrm{DL}}(x_0,s)\mathbb{E}_{\Psi_B}\left[\prod_{i,b_i\in\Psi_B\setminus\{b_0\}}\kappa^{\mathrm{DL}}(x_i,s)\right],\end{aligned} \tag{48}$$

where $\kappa^{\mathrm{DL}}(\cdot)$ is given in (17) and (a) is from the same method in (43). Applying the PGFL of PPP [35] into (48), we have

$$\mathcal{L}_{W^{\mathrm{DL}}|x_0}(s) = \kappa^{\mathrm{DL}}(x_0,s) \times \exp\left(-2\pi\lambda_B\int_{x_0}^\infty\left[1-\kappa^{\mathrm{DL}}(x,s)\right]x\,\mathrm{d}x\right), \tag{49}$$

where $\lambda_B = \lambda_b\exp(-\lambda_r R^2)$. Following the result of (46), we complete the proof of Theorem 3 by replacing $\mathcal{L}_{W^{\mathrm{DL}}}(s)$ with $\mathcal{L}_{W^{\mathrm{DL}}|x_0}(s)$.

References

[1] F. Boccardi, R. W. Heath Jr., A. Lozano, T. L. Marzetta, and P. Popovski, "Five disruptive technology directions for 5G," *IEEE Commun. Mag.*, vol. 52, no. 2, pp. 74–80, Feb. 2014.

[2] *Switzerland Halts Rollout of 5G Over Health Concerns*. Accessed: Feb. 18, 2020. [Online]. Available: https://www.ft.com/content/848c5b44-4d7a-11ea-95a0-43d18ec715f5

[3] U. Bergqvist, J. H. Bernhardt, J. P. Cesarini, M. Grandolfo, M. Hietanen, and A. F. Mckinlay, "Guidelines for limiting exposure to time-varying electric, magnetic, and electromagnetic fields (up to 300 GHz)," *Health Phys.*, vol. 74, no. 4, pp. 494–522, Apr. 1998.

[4] International Commission on Non-Ionizing Radiation Protection (ICNIRP). (Mar. 2020). *ICNIRP Guidelines on Limiting Exposure to Time-Varying Electric, Magnetic and Electromagnetic Fields (100 kHz to 300 GHz)*. [Online]. Available: https://www.icnirp.org/cms/upload/publications/ICNIRPrfgdl2020.pdf

[5] Y. A. Sambo, F. Heliot, and M. A. Imran, "A survey and tutorial of electromagnetic radiation and reduction in mobile communication systems," *IEEE Commun. Surveys Tuts.*, vol. 17, no. 2, pp. 790–802, 2nd Quart., 2014.

[6] K.-H. Ng, "Non-ionizing radiations–sources, biological effects, emissions and exposures," in *Proc. Int. Conf. Non-Ionizing Radiat.*, 2003, pp. 1–16.

[7] K. R. Foster, M. C. Ziskin, Q. Balzano, and A. Hirata, "Thermal analysis of averaging times in radio-frequency exposure limits above 1 GHz," *IEEE Access*, vol. 6, pp. 74536–74546, 2018.

[8] D. Belpomme, L. Hardell, I. Belyaev, E. Burgio, and D. O. Carpenter, "Thermal and non-thermal health effects of low intensity non-ionizing radiation: An international perspective," *Environ. Pollut.*, vol. 242, pp. 643–658, Jan. 2018.

[9] *Guidance on Complying With Limits for Human Exposure to Electromagnetic Fields*, ITU-T, Geneva, Switzerland, 2021.

[10] *Human Exposure to Radiofrequency Electromagnetic Fields and Reassessment of FCC Radiofrequency Exposure Limits and Policies. A Rule by the Federal Communications Commission on 04/01/2020 Published in: The Federal Register; 2020*, Federal Communications Commission, Washington, DC, USA, 2020.

[11] World Health Organization. *Exposure Limits for Radio-Frequency Fields (Public)—Data by Country*. Accessed: May 19, 2020. [Online]. Available: https://apps.who.int/gho/data/view.main.EMFLIMITSPUBCRADIOFREQUENCYv

[12] The Communications and Information Technology Commission (CITC). (2021). *Regulations on Exposure to EMF*. [Online]. Available: https://www.citc.gov.sa/ar/new/publicConsultation/Documents/ExposuretoEMF_AR_EN.pdf

[13] H. Chiang. (2009). *Rationale for Setting EMF Exposure Standards*. Accessed: May 19, 2020. [Online]. Available: https://www.salzburg.gv.at/gesundheit_/Documents/proceedings_(20)_chiang.pdf

[14] *Electromagnetic Fields Generated by Electrical Products and Telecommunication Devices (Hong Kong Regulation)*. Accessed: May 19, 2020. [Online]. Available: https://www.info.gov.hk/gia/general/201212/12/P201212120306.htm

[15] *Liechtenstein Reduces RF Exposure Limits*. Accessed: May 19, 2020. [Online]. Available: http://www.emfrf.com/liechtenstein-reduces-RF-exposure-limits/

[16] T. B. of Supervisors of the County of San Diego. (2019). *Ordinance NO. 10622 (New Series)*. [Online]. Available: https://tinyurl.com/2p8rr35v

[17] *Toxicology and Carcinogenesis Studies in HSD: Sprague Dawley SD Rats Exposed to Whole-Body Radio Frequency Radiation at a Frequency (900 MHz) and Modulations (GSM and CDMA) Used by Cell Phones*, National Toxicology Program, US Department of Health and Human Services, Washington, DC, USA, 2018.

[18] S. Wall, T. Kendig, D. Dobraca, and M. Lipsett, "Real-world cell phone radiofrequency electromagnetic field exposures," *Environ. Res.*, vol. 171, pp. 581–592, Apr. 2019. [Online]. Available: http://www.sciencedirect.com/science/article/pii/S0013935118305024

[19] Y. Huang et al., "Comparison of average global exposure of population induced by a macro 3G network in different geographical areas in France and Serbia," *Bioelectromagnetics*, vol. 37, no. 6, pp. 382–390, 2016.

[20] R. Pawlak, P. Krawiec, and J. Z. Urek, "On measuring electromagnetic fields in 5G technology," *IEEE Access*, vol. 7, pp. 29826–29835, 2019.

[21] L. Chiaraviglio et al., "Massive measurements of 5G exposure in a town: Methodology and results," *IEEE Open J. Commun. Soc.*, vol. 2, pp. 2029–2048, 2021.

[22] S. Aerts et al., "In-situ measurement methodology for the assessment of 5G NR massive MIMO base station exposure at sub-6 GHz frequencies," *IEEE Access*, vol. 7, pp. 184658–184667, 2019.

[23] L. Chiaraviglio, S. Turco, G. Bianchi, and N. Blefari-Melazzi, "Do dense 5G networks increase exposure to electromagnetic fields?" *Proc. IEEE*, vol. 109, no. 12, pp. 1880–1887, Dec. 2021.

[24] Q. Gontier et al., "A stochastic geometry approach to EMF exposure modeling," *IEEE Access*, vol. 9, pp. 91777–91787, 2021.

[25] M. A. Hajj, S. Wang, L. T. Tu, S. Azzi, and J. Wiart, "A statistical estimation of 5G massive MIMO networks' exposure using stochastic geometry in mmWave bands," *Appl. Sci.*, vol. 10, no. 23, p. 8753, Dec. 2020.

[26] A. Elzanaty, L. Chiaraviglio, and M.-S. Alouini, "5G and EMF exposure: Misinformation, open questions, and potential solutions," *Frontiers Commun. Netw.*, vol. 2, Apr. 2021, Art. no. 635716.

[27] L. Chiaraviglio, A. Elzanaty, and M.-S. Alouini, "Health risks associated with 5G exposure: A view from the communications engineering perspective," *IEEE Open J. Commun. Soc.*, vol. 2, pp. 2131–2179, 2021.

[28] H. Ibraiwish, A. Elzanaty, Y. H. Al-Badarneh, and M.-S. Alouini, "EMF-aware cellular networks in RIS-assisted environments," *IEEE Commun. Lett.*, vol. 26, no. 1, pp. 123–127, Jan. 2022.
[29] A. Subhash, A. Kammoun, A. Elzanaty, S. Kalyani, Y. H. Al-Badarneh, and M.-S. Alouini, "Max-min data rate optimization for RIS-aided uplink communications with green constraints," 2023, *arXiv:2208.00182*.
[30] A. Subhash, A. Kammoun, A. Elzanaty, S. Kalyani, Y. H. Al-Badarneh, and M.-S. Alouini, "Optimal phase shift design for fair allocation in RIS aided uplink network using statistical CSI," 2022, *arXiv:2209.08983*.
[31] S. Javed, A. Elzanaty, O. Amin, M.-S. Alouini, and B. Shihada, "EMF-aware probabilistic shaping design for hardware-distorted communication systems," *Frontiers Commun. Netw.*, vol. 3, pp. 1–10, May 2022.
[32] N. A. Muhammad, N. Seman, N. I. A. Apandi, C. T. Han, Y. Li, and O. Elijah, "Stochastic geometry analysis of electromagnetic field exposure in coexisting sub-6 GHz and millimeter wave networks," *IEEE Access*, vol. 9, pp. 112780–112791, 2021.
[33] Z. Lou, A. Elzanaty, and M.-S. Alouini, "Green tethered UAVs for EMF-aware cellular networks," *IEEE Trans. Green Commun. Netw.*, vol. 5, no. 4, pp. 1697–1711, Dec. 2021.
[34] M. Nemati, J. Park, and J. Choi, "RIS-assisted coverage enhancement in millimeter-wave cellular networks," *IEEE Access*, vol. 8, pp. 188171–188185, 2020.
[35] J. G. Andrews, A. K. Gupta, and H. S. Dhillon, "A primer on cellular network analysis using stochastic geometry," 2016, *arXiv:1604.03183*.
[36] M. Haenggi, *Stochastic Geometry for Wireless Networks*. Cambridge, U.K.: Cambridge Univ. Press, 2012.
[37] M. K. Simon and M.-S. Alouini, *Digital Communication Over Fading Channels*, vol. 95. Hoboken, NJ, USA: Wiley, 2005.
[38] P. J. Davis, "Leonhard Euler's integral: A historical profile of the gamma function: In memoriam: Milton Abramowitz," *Amer. Math. Monthly*, vol. 66, no. 10, pp. 849–869, 1959.
[39] *Electromagnetic Field Compliance Assessments for 5G Wireless Networks*, Standard ITU-T K.Sup16 (05/19), International Telecommunication Union (ITU), May 2019. [Online]. Available: http://handle.itu.int/11.1002/1000/13938
[40] J. Gil-Pelaez, "Note on the inversion theorem," *Biometrika*, vol. 38, no. 3, pp. 481–482, Dec. 1951.
[41] L. Chiaraviglio et al., "Planning 5G networks under EMF constraints: State of the art and vision," *IEEE Access*, vol. 6, pp. 51021–51037, 2018.
[42] S. Kuehn, S. Pfeifer, B. Kochali, N. Kuster, and C. Bern, "Modelling of total exposure in hypothetical 5G mobile networks for varied topologies and user scenarios," Swiss Federal Office Environ. (FOEN), Ittigen, Switzerland, Tech. Rep., 816, 2019.
[43] L. Chiaraviglio, C. Lodovisi, S. Bartoletti, A. Elzanaty, and M.-S. Alouini, "Dominance of smartphone exposure in 5G mobile networks," 2022, *arXiv:2211.01077*.
[44] G. Vermeeren et al., "Low EMF exposure future networks D2.8 global wireless exposure metric definition," LEXNET Consortium, Moulineaux, France, Tech. Rep., 2, 2015.
[45] A. Eiger, K. Sikorski, and F. Stenger, "A bisection method for systems of nonlinear equations," *ACM Trans. Math. Softw.*, vol. 10, no. 4, pp. 367–377, 1984.
[46] J. Kiefer, "Sequential minimax search for a maximum," *Proc. Amer. Math. Soc.*, vol. 4, no. 3, pp. 502–506, 1953.
[47] *Further Advancements for E-Utra Physical Layer Aspects*, document 36, 3GPP Technical Specification TR, 2010.
[48] H. ElSawy, A. Sultan-Salem, M. S. Alouini, and M. Z. Win, "Modeling and analysis of cellular networks using stochastic geometry: A tutorial," *IEEE Commun. Surveys Tuts.*, vol. 19, no. 1, pp. 167–203, 1st Quart., 2017.
[49] J. G. Andrews, F. Baccelli, and R. K. Ganti, "A tractable approach to coverage and rate in cellular networks," *IEEE Trans. Commun.*, vol. 59, no. 11, pp. 3122–3134, Oct. 2011.

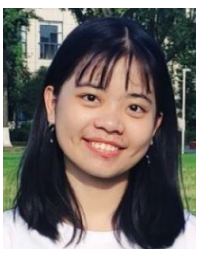

Lin Chen received the B.S. degree in communication engineering from the University of Electronic Science and Technology of China (UESTC) in 2022. She is currently pursuing the Ph.D. degree with the Department of Information Engineering, The Chinese University of Hong Kong (CUHK). From 2021 to 2022, she was a Visiting Student at the KAUST. Her research interests include UAV, RIS, and deep learning (DL) for wireless communications.

Ahmed Elzanaty (Senior Member, IEEE) received the Ph.D. degree (cum laude) in electronics, telecommunications, and information technology from the University of Bologna, Italy, in 2018. Currently, he is a Lecturer (Assistant Professor) with the Institute for Communication Systems, University of Surrey, U.K. Before that, he was a Post-Doctoral Fellow at the King Abdullah University of Science and Technology (KAUST), Saudi Arabia. He has participated in several national and European projects, such as GRETA and EuroCPS. His research interests include the design and performance analysis of wireless communications and localization systems.

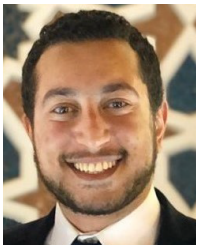

Mustafa A. Kishk (Member, IEEE) received the B.Sc. and M.Sc. degrees in electrical engineering from Cairo University, Giza, Egypt, in 2013 and 2015, respectively, and the Ph.D. degree in electrical engineering from Virginia Tech, Blacksburg, VA, USA, in 2018. He is currently an Assistant Professor at the Electronic Engineering Department, Maynooth University, Ireland. Before that, he was a Post-Doctoral Research Fellow with the Communication Theory Laboratory, King Abdullah University of Science and Technology, Saudi Arabia. His current research interests include stochastic geometry, UAV-enabled communication systems, and satellite-enabled communications. He was a recipient of the IEEE ComSoc Outstanding Young Researcher Award for Europe, Middle East, and Africa Region, in 2022. He also serves as an Associate Editor for the IEEE WIRELESS COMMUNICATIONS LETTERS. He was recognized as an Exemplary Reviewer by the IEEE COMMUNICATIONS LETTERS in 2020 and 2021.

Luca Chiaraviglio (Senior Member, IEEE) received the Ph.D. degree in telecommunication and electronics engineering from the Polytechnic University of Turin, Italy. He is currently an Associate Professor with the University of Rome "Tor Vergata," Italy, teaching the courses of the "Internet of Things" and "Networking and Internet." He has coauthored more than 160 papers published in international journals, books, and conferences. His current research interests include 6G networks, electromagnetic fields assessments of 5G networks, and health risks assessment of 5G communications. He received the Best Paper Award at the IEEE Vehicular Technology Conference (VTC Spring) in 2020 and 2016, and at the Conference on Innovation in Clouds, Internet and Networks (ICIN) in 2018, all of them appearing as the first author. Some of his papers are listed as the Best Readings on Green Communications by the IEEE. Moreover, he has been recognized as an author in the top 1% most highly cited papers in the information and communication technology (ICT) field worldwide and top 2% world scientists according to the 2021 and 2022 updates of the science-wide author databases of standardized citation indicators.

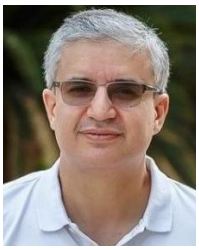

Mohamed-Slim Alouini (Fellow, IEEE) was born in Tunis, Tunisia. He received the Ph.D. degree in electrical engineering from the California Institute of Technology (Caltech), Pasadena, CA, USA, in 1998. He worked as a Faculty Member with the University of Minnesota, USA, and Texas A&M University at Qatar, Qatar, before joining KAUST, Saudi Arabia, as a Professor of electrical engineering, in 2009. His current research interests include the modeling, design, and performance analysis of wireless communication systems.